Progress in first-principles simulation of SOL plasma turbulence and neutral atom dynamics with the GBS code

P. Ricci[1], F. Halpern[1], J. Loizu[2], S. Jolliet[1], R. Jorge[1,3], J. Morales[1], A. Mosetto[1], P. Paruta[1], F. Riva[1] and C. Wersal[1]

[1]Swiss Plasma Center (SPC), Ecole Polytechnique Fédérale de Lausanne (EPFL), CH-1015 Lausanne, Switzerland
[2]Max-Planck-Princeton Center for Plasma Physics, Wendelsteinstraße 1, D-17491 Greifswald, Germany
[3]Instituto de Plasmas e Fusão Nuclear, Instituto Superior Técnico, Universidade de Lisboa, 1049-001 Lisboa, Portugal

Corresponding Author: paolo.ricci@epfl.ch

Abstract:
The GBS code was developed in the last few years to simulate plasma turbulence in SOL conditions. GBS advances the drift-reduced Braginskii equations for low-frequency plasma turbulence, solving at the same time a kinetic equation for the neutral atoms by the method of characteristics. The interaction of the plasma with the neutrals is taken self-consistently into account, by evaluating plasma source and energy losses due to ionization events, the drag due to charge-exchange collisions, and the recombination processes. GBS verification was performed by using the method of manufactured solutions, and its results have been validated against experimental data from several tokamaks worldwide, showing good agreement. In the present work, we focus on our recent insights on the neutral atom dynamics. We first illustrate the model that allows us to evolve at the same time plasma turbulence and neutral atom dynamics. Second, we describe our recent progress in the study of the transition from the sheath- to the conduction-limited regimes that was simulated in GBS by increasing the plasma density in the system. Thanks to the simulation results, we expanded and refined the so-called two-point model that is used to estimate the drop of electron and ion temperature along the magnetic field lines in the SOL. We also report on the most recent GBS research activities targeted to increase the flexibility of GBS, that allowed us to study the effect of shaping (e.g., elongation and triangularity) on the SOL width and to uncover the physics at play at the interface with the closed flux surface region.

1 Introduction

The interaction between neutral dynamics and turbulence in the SOL is a largely unexplored area of research, despite the fact that it has critical consequences for fuelling, confinement, and level of heat load onto the vessel. For example, the steady-state heat

load onto the vessel constrains the lifetime of the plasma facing components of tokamak devices and regulate the level of impurities in the core, two critical issues on the way towards a fusion reactor. The heat load depends on the scrape-off layer (SOL) width [1], which results from a balance between plasma outflowing from the core region, turbulent transport, and losses to the divertor or limiter, and involves a complex interaction of the neutral atoms with the plasma. Understanding the interaction between plasma turbulence and neutral atom dynamics in the SOL is therefore crucial for the operation of ITER and beyond.

The GBS code has been developed in the last few years to simulate plasma turbulence in SOL conditions [2, 3]. GBS advances the drift-reduced Braginskii equations for low-frequency plasma turbulence [4], solving at the same time a kinetic equation for the neutral atoms by the method of characteristics [5]. In GBS the plasma dynamics is evolved as the interplay between plasma sources (due to the neutral ionization and the plasma outflow from the tokamak core), turbulent transport, and plasma losses (at the limiter or divertor plates or through recombination processes). The simulations evolve self-consistently both the plasma profile and its fluctuations, with no separation between the equilibrium and fluctuations. A detailed study of the interaction of the plasma with the solid wall was carried out in order to implement correctly the physics of this region in GBS [6]. The plasma wall interaction was modeled by using a fully kinetic code and, based on the kinetic results, a set of boundary conditions was found that were implemented in GBS at the sheath edge, where the drift-reduced Braginskii model loses its validity. The neutral module implemented in GBS represents the first-ever successful implementation of a self-consistent neutral solver within a first-principles turbulence code [5]. The interaction of the plasma with the neutrals is taken self-consistently into account, by evaluating the plasma source and energy losses due to ionization events, the drag due to charge-exchange collisions, and the recombination processes.

In the past, thanks to the GBS simulations and analytical investigations, we have reached an understanding of the mechanisms leading to SOL turbulent saturation [7], which allowed us to estimate the scaling of the SOL width in limited discharges in good agreement with experiments [8]. We have also pointed out the SOL turbulent regimes [9], the role of electromagnetic effects [10], the mechanisms determining the SOL electrostatic potential [11], the phenomena responsible for the SOL intrinsic toroidal rotation [12], the role of finite aspect ratio effects [13], and the impact of the limiter position [14].

In the present work, we focus on our recent insights on the neutral atom dynamics. We first illustrate the model that allows us to evolve at the same time plasma turbulence and neutral atom dynamics. We then describe some of our recent simulation results that point out the impact of the neutral atom dynamics on the SOL profiles. We finally report on the progress we carried out to increase the flexibility of GBS. In fact, GBS simulations focused on the simplest circular limited configuration, as a stepping stone towards more complicated configurations. Now, we have started to study turbulence in more advanced geometries. The effect of shaping (e.g., elongation and triangularity) on the SOL width was simulated and analyzed. The GBS simulation domain was extended inside the last-closed flux surface. Moreover, in parallel to a new multi-grid solver that significantly improved the parallelization of GBS [3], a more flexible numerical scheme

is being implemented that will enable simulations of medium size tokamaks in diverted geometries.

2 Model equations

In the SOL the plasma dynamics results from the interplay of the plasma sources (due to the neutral ionization and the plasma outflow from the tokamak core), turbulent transport, and plasma losses (at the limiter or divertor plates or through recombination processes). Therefore, a model has to evolve self-consistently both the plasma profile and its fluctuations, with no separation between the equilibrium and fluctuation scale lengths.

The perpendicular (turbulent) dynamics occurs on time scales longer than the ion cyclotron period, and it has length scales of the order of ρ_s, while the relevant length scale for the parallel dynamics is the magnetic field line length $\sim R$. Hence, it is advantageous to eliminate the undesired (fast) temporal scales, and to separate the parallel and the perpendicular dynamics. The required separation of temporal and spatial scales is achieved through the use of the following velocity representation:

$$\mathbf{v}_e = v_{\|e}\hat{\mathbf{b}} + \mathbf{v}_{\mathbf{E}\times\mathbf{B}} + \mathbf{v}_{\star,e} \tag{1}$$

$$\mathbf{v}_i = v_{\|i}\hat{\mathbf{b}} + \mathbf{v}_{\mathbf{E}\times\mathbf{B}} + \mathbf{v}_{\star,i} + \mathbf{v}_{\mathrm{pol},i} \tag{2}$$

together with the approximation $\mathbf{E} = -\nabla\phi - \hat{\mathbf{b}}_0\partial_t\psi$, where ψ represents the perturbed poloidal magnetic flux. The drift velocities $\mathbf{v}_{\mathbf{E}\times\mathbf{B}} = -\nabla\phi \times \hat{\mathbf{b}}_0/B$ and $\mathbf{v}_{\star,e,i} = -\nabla p_{e,i} \times \hat{\mathbf{b}}_0/(Z_{e,i}en_{e,i}B)$ are the zeroth order solution to the perpendicular component of the moment equations, $\hat{\mathbf{b}}$ is a unit vector in the direction of the magnetic field and $\hat{\mathbf{b}}_0$ its equilibrium direction. The ion polarization drift $\mathbf{v}_{\mathrm{pol},i}$ is obtained as a first order correction to $\mathbf{v}_i$.

We retain an equation for the electron density, a vorticity equation that enforces charge conservation, and equations for the ion and electron temperatures and parallel velocities:

$$\frac{\partial n}{\partial t} = -\frac{1}{B}[\phi, n] - \nabla(nv_{\|\mathrm{e}}\hat{\mathbf{b}}) + \frac{2}{eB}\left[C(p_\mathrm{e}) - enC(\phi)\right] + \mathcal{D}_\mathrm{n}(n) + S_\mathrm{n} + n_\mathrm{n}\nu_\mathrm{iz} - n\nu_\mathrm{rec} \tag{3}$$

$$\frac{\partial \tilde{\omega}}{\partial t} = -\frac{1}{B}[\phi, \tilde{\omega}] - v_{\|\mathrm{i}}\nabla_\|\tilde{\omega} + \frac{B^2}{m_\mathrm{i}n}\nabla(j_\|\hat{\mathbf{b}}) + \frac{2B}{m_\mathrm{i}n}C(p) + \mathcal{D}_{\tilde{\omega}}(\tilde{\omega}) - \frac{n_\mathrm{n}}{n}\nu_\mathrm{cx}\tilde{\omega} \tag{4}$$

$$\begin{aligned}\frac{\partial v_{\|\mathrm{e}}}{\partial t} + \frac{e}{m_\mathrm{e}}\frac{\partial \Psi}{\partial t} = &-\frac{1}{B}[\phi, v_{\|\mathrm{e}}] - v_{\|\mathrm{e}}\nabla_\| v_{\|\mathrm{e}} + \frac{e}{\sigma_\| m_\mathrm{e}}j_\| + \frac{e}{m_\mathrm{e}}\nabla_\|\phi - \frac{T_\mathrm{e}}{m_\mathrm{e}n}\nabla_\| n - \frac{1.71}{m_\mathrm{e}}\nabla_\| T_\mathrm{e} + \mathcal{D}_{v_{\|\mathrm{e}}}(v_{\|\mathrm{e}}) \\ &+ \frac{n_\mathrm{n}}{n}(\nu_\mathrm{en} + 2\nu_\mathrm{iz})(v_{\|\mathrm{n}} - v_{\|\mathrm{e}})\end{aligned} \tag{5}$$

$$\frac{\partial v_{\parallel \mathrm{i}}}{\partial t} = -\frac{1}{B}[\phi, v_{\parallel \mathrm{i}}] - v_{\parallel \mathrm{i}}\nabla_\parallel v_{\parallel \mathrm{i}} - \frac{1}{m_\mathrm{i} n}\nabla_\parallel p + \mathcal{D}_{v_{\parallel \mathrm{i}}}(v_{\parallel \mathrm{i}}) + \frac{n_\mathrm{n}}{n}(\nu_\mathrm{iz} + \nu_\mathrm{cx})(v_{\parallel \mathrm{n}} - v_{\parallel \mathrm{i}}) \tag{6}$$

$$\frac{\partial T_\mathrm{e}}{\partial t} = -\frac{1}{B}[\phi, T_\mathrm{e}] - v_{\parallel \mathrm{e}}\nabla_\parallel T_\mathrm{e} + \frac{4T_\mathrm{e}}{3eB}\left[\frac{T_\mathrm{e}}{n}C(n) + \frac{7}{2}C(T_\mathrm{e}) - eC(\phi)\right] + \frac{2T_\mathrm{e}}{3n}\left[\frac{0.71}{e}\nabla(j_\parallel \hat{\mathbf{b}}) - n\nabla(v_{\parallel \mathrm{e}}\hat{\mathbf{b}})\right] + \mathcal{D}_{T_\mathrm{e}}(T_\mathrm{e}) + \mathcal{D}^\parallel_{T_\mathrm{e}}(T_\mathrm{e}) + S_{T_\mathrm{e}} + \frac{n_\mathrm{n}}{n}\nu_\mathrm{iz}\left[-\frac{2}{3}E_\mathrm{iz} - T_\mathrm{e} + m_\mathrm{e}v_{\parallel \mathrm{e}}\left(v_{\parallel \mathrm{e}} - \frac{4}{3}v_{\parallel \mathrm{n}}\right)\right] - \frac{n_\mathrm{n}}{n}\nu_\mathrm{en}m_\mathrm{e}\frac{2}{3}v_{\parallel \mathrm{e}}(v_{\parallel \mathrm{n}} - v_{\parallel \mathrm{e}}) \tag{7}$$

$$\frac{\partial T_\mathrm{i}}{\partial t} = -\frac{1}{B}[\phi, T_\mathrm{i}] - v_{\parallel \mathrm{i}}\nabla_\parallel T_\mathrm{i} + \frac{4T_\mathrm{i}}{3eB}\left[C(T_\mathrm{e}) + \frac{T_\mathrm{e}}{n}C(n) - \frac{5}{2}C(T_\mathrm{i}) - eC(\phi)\right] + \frac{2T_\mathrm{i}}{3n}\left[\frac{1}{e}\nabla(j_\parallel \hat{\mathbf{b}}) - n\nabla(v_{\parallel \mathrm{i}}\hat{\mathbf{b}})\right] + \mathcal{D}_{T_\mathrm{i}}(T_\mathrm{i}) + \mathcal{D}^\parallel_{T_\mathrm{i}}(T_\mathrm{i}) + S_{T_\mathrm{i}} + \frac{n_\mathrm{n}}{n}(\nu_\mathrm{iz} + \nu_\mathrm{cx})\left[T_\mathrm{n} - T_\mathrm{i} + \frac{1}{3}(v_{\parallel \mathrm{n}} - v_{\parallel \mathrm{i}})^2\right] \tag{8}$$

with $p = n(T_\mathrm{e} + T_\mathrm{i})$, the total pressure, and $\sigma_\parallel = 1.96e^2 n\tau_\mathrm{e}/m_\mathrm{e}$, the parallel conductivity, where τ_e is the electron collision time. The generalized vorticity, $\tilde{\omega} = \omega + 1/e\nabla^2_\perp T_\mathrm{i}$, is related to the electrostatic potential by $\nabla^2_\perp \phi = \omega$, while $(\beta_{\mathrm{e}0}/2)\nabla^2_\perp \Psi = j_\parallel$, with $\beta_{\mathrm{e}0} = 2\mu_0 p_\mathrm{e}/B^2$ and $j_\parallel = n\left(v_{\parallel i} - v_{\parallel e}\right)$. The following operators have been introduced $\nabla_\parallel A = \hat{\mathbf{b}}\cdot\nabla A$, $[A, B] = \hat{\mathbf{b}}_0\cdot(\nabla A \times \nabla B)$, and $C(A) = B/2[\nabla \times (\hat{\mathbf{b}}_0/B)]\cdot\nabla A$. The ionization, recombination, elastic electron-neutral, and charge-exchange processes are described, respectively, through the use of Krook operators with collision frequencies defined as $\nu_\mathrm{iz} = n_e\langle v_e\sigma_\mathrm{iz}(v_e)\rangle$, $\nu_\mathrm{rec} = n_e\langle v_e\sigma_\mathrm{rec}(v_e)\rangle$, $\nu_\mathrm{en} = n_e\langle v_e\sigma_\mathrm{en}(v_e)\rangle$, $\nu_\mathrm{cx} = n_i\langle v_i\sigma_\mathrm{cx}(v_i)\rangle$ where σ_iz, σ_rec, σ_en and σ_cx, are the ionization, recombination, elastic electron-neutral, and charge-exchange cross sections. The neutral atoms dynamics is obtained by solving the kinetic equation

$$\frac{\partial f_\mathrm{n}}{\partial t} + \mathbf{v}\cdot\frac{\partial f_\mathrm{n}}{\partial \mathbf{x}} = -\nu_\mathrm{iz}f_\mathrm{n} - \nu_\mathrm{cx}\left(f_\mathrm{n} - \frac{n_\mathrm{n}}{n_i}f_i\right) + \nu_\mathrm{rec}f_i. \tag{9}$$

In Eq. (4), the polarization velocity and its divergence retain corrections due to density gradients, *i.e.* the commonly used Boussinesq approximation is avoided. The source terms S_n, S_{T_e}, and S_{T_i} have been added to the density and temperature equations to model the outflow of hot plasma from the core to the SOL. A detailed study of the interaction of the plasma with the solid wall was carried out and, based on the kinetic results, a set of boundary conditions was found, implemented in GBS at the sheath edge [6].

3 Numerical implementation

A radial section of a torus, with coordinate system $(y = a\theta, x, \varphi)$ is mapped to a discrete Cartesian grid. The φ coordinate is periodic, while periodicity in y can be selected for

a chosen range of x – thus, we can vary between a poloidally periodic plasma, a limited plasma, or we can mix open and closed field lines. Time integration is carried out with the Runge-Kutta order 4 algorithm.

Spatial gradients are computed using standard second order centered finite difference formulas, while the $\mathbf{E} \times \mathbf{B}$ non-linear advection terms are discretized using the Arakawa scheme. The Poisson and Ampère equations can be solved using sparse matrix methods, or using a stencil-based multigrid solver. The kinetic equation for the neutral atoms is solved by using the method of characteristics.

The verification of the correct implementation and solution of the model equations was performed by using the method of manufactured solutions [15]. A thorough benchmark of GBS results was also performed against a number of other turbulence codes and experimental results from basic plasma physics experiments [16]. Detailed comparisons with gas puff imagining from Alcator C-Mod were carried out with remarkable success [17].

4 Simulation results

Figures 1 and 2 show typical snapshots of plasma density, parallel electron and ion velocities, electron and ion temperatures, electrostatic potential, neutral density, and ionization source, $S_{iz} = n_n \nu_{iz}$, on a poloidal cross-section. These snapshots are taken when turbulence is fully developed during the saturated state of two simulations, at low and high density. T he poloidal dependence of the relevant plasma quantities (plasma density, electron and ion parallel velocities, electron and ion temperatures, electrostatic potential, neutral density, and S_{iz}) for the low- and high-density simulations are shown in Fig. 3. The displayed profiles are averaged over a time window of 20 R/c_{s0}, over the full toroidal angle, and over a radial region extending for 20 ρ_{s0}, centered at a distance of 30 ρ_{s0} from the separatrix. We point out a few interesting differences between the high- and low-density simulations. The poloidal density profile in the high-density simulation is flatter than in the low-density simulation. This is due to the fact that the plasma source due to the ionizations occurring close to the limiter inside the SOL is much higher in the high-density simulation, preventing the plasma density to drop when approaching the sheaths. The parallel velocity profiles

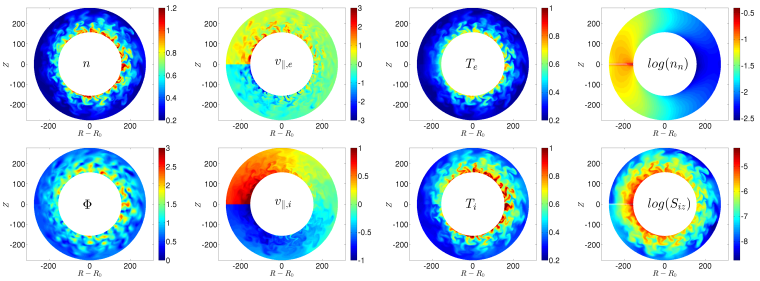

FIG. 1: Snapshots on a poloidal cross-section of plasma density, electric potential, ion and electron parallel velocities, electron and ion temperatures, neutral density, and the ionization source term, S_{iz}, for a low-density simulation with density at the last closed flux surface $n_0 = 5 \cdot 10^{18} m^{-3}$.

(which are expected to be approximately linear if the plasma source is poloidally constant) are somewhat flatter close to the limiter in the high-density scenario; however, the flattening is not particularly significant, because a relatively large fraction of the plasma density source is still due to the poloidally constant outflow of particles from the core.

Furthermore, both electron and ion temperature poloidal gradients increase in the high-density scenario, which is expected while going towards the conduction limited regime. The mechanisms that lead to this temperature drop include the reduced parallel heat conductivity (due to lower temperature and higher density), and the direct energy loss due to ionizations (see, e.g., Ref. [18]).

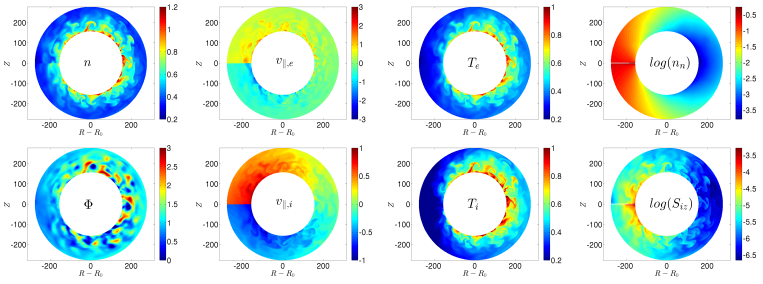

FIG. 2: Same as in Fig. 1, with $n_0 = 5 \cdot 10^{19} m^{-3}$.

5 Implementation of a flexible numerical algorithm

Studies carried out using GBS simulations have helped provide an understanding of the turbulence saturation mechanisms in the SOL, the non-linear turbulent regimes, the scaling of the tokamak SOL width, the role of electromagnetic effects, and the equilibrium electric field. The code was designed around a simple, robust, and scalable numerical scheme, based in particular on a field-aligned approach. This allowed us to simulate the SOL of medium size tokamaks such as TCV or Alcator C-Mod at a cost affordable on today's high-performance computers. This numerical approach constrained the GBS simulation to limited configuration, with a radially con-

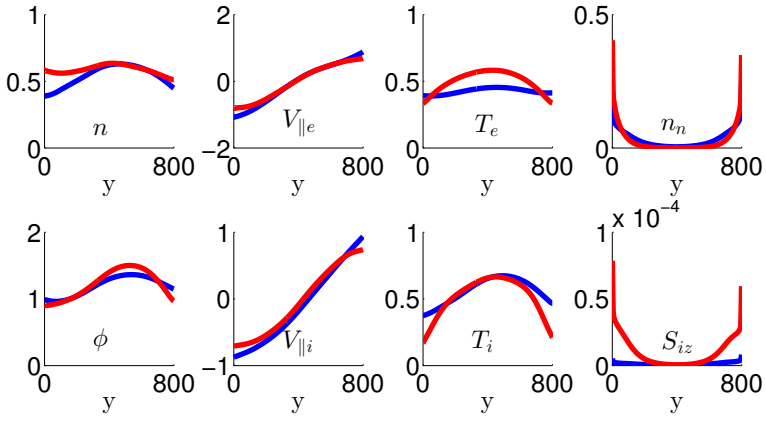

FIG. 3: Time-averaged poloidal profiles of plasma density, electric potential, ion and electron parallel velocities, electron and ion temperatures, neutral density, and the ionization source term, S_{iz}*, for the low (blue) and high (red) plasma density scenario. Quantities are normalised to their values at the last closed flux surface.*

stant safety factor.

We have now implemented a non- field-aligned approach in GBS [19]. The properties of this numerical algorithm were tested on the propagation of shear-Alfvn waves. The parallel derivatives are computed by adding the derivatives along the poloidal and toroidal directions, which are evaluated with a fourth-order finite difference algorithm. The new scheme has been applied to limited tokamaks with radially varying safety factor profiles, and, diverted configurations with an X point.

This research was supported in part by the Swiss National Science Foundation and was carried out within the framework of the EUROfusion Consortium. It received funding from the Euratom research and training programme 2014-2018 under grant agreement No 633053. The views and opinions expressed herein do not necessarily reflect those of the European Commission.

References

[1] W. Fundamenski et al, Nucl. Fusion 51 (2011) 093028; T. Eich et al, Phys. Rev. Lett. 107 (2012) 215001; J. Gunn et al, J. Nucl. Mater. 438 (2013) S184; M.A. Makowski et al, Phys. Plasmas 19 (2012) 056122.

[2] P. Ricci et al, Plasma Phys. Contr. Fusion 54 (2012) 124047

[3] F.D. Halpern et al, J. Comp. Physics, 315 (2016) 388.

[4] A. Zeiler et al, Phys. Plasmas 5 (1998) 2654.

[5] C. Wersal and P. Ricci, Nucl. Fusion 55, (2015) 123014.

[6] J. Loizu et al, Phys. Plasmas 19, (2012) 122307.

[7] P. Ricci et al., Phys. Plasmas 20 (2013) 010702.

[8] F.D. Halpern et al, Nucl. Fusion 53, (2013) 122001; F.D. Halpern et al, Nucl. Fusion 54, (2014) 043003.

[9] A. Mosetto et al, Phys. Plasmas 20, (2013) 092308; A. Mosetto et al, Phys. Plasmas 22, (2015) 012308.

[10] F.D. Halpern et al, Phys. Plasmas 20, (2013) 052306.

[11] J. Loizu et al, Plasma Phys. Contr. Fusion 55 (2013) 124019.

[12] J. Loizu et al, Phys. Plasmas 21 (2014) 062309.

[13] S. Jolliet et al, Phys. Plasmas 21 (2014) 022303.

[14] J. Loizu et al, Nucl. Fusion 54 (2014) 083033.

[15] F. Riva et al, Phys. Plasmas 21, (2014) 062301.

[16] F. Riva et al, Plasma Phys. Contr. Fusion 58, (2016) 044005.

[17] F.D. Halpern et al, Plasma Phys. Contr. Fusion 57, (2015) 054005.

[18] P. Stangeby, The plasma boundary of magnetic fusion devices (2000) IOP Publishing.

[19] S. Jolliet et al, Comp. Phys. Comm. 188, (2015) 21.